Journal of Biomechanics 47 (2014) 3613–3621

Contents lists available at ScienceDirect

Journal of Biomechanics

journal homepage: www.elsevier.com/locate/jbiomech
www.JBiomech.com

Hybrid neuromusculoskeletal modeling to best track joint moments using a balance between muscle excitations derived from electromyograms and optimization

Massimo Sartori [a,*], Dario Farina [a], David G. Lloyd [b,c]

[a] Department of Neurorehabilitation Engineering, University Medical Center Goettingen, Georg-August University, Goettingen, Germany
[b] Centre for Musculoskeletal Research, Griffith Health Institute, Griffith University, Southport, QLD, Australia
[c] Faculty of Science and Faculty of Engineering, University of Western Australia, Crawley, WA, Australia

ARTICLE INFO

Article history:
Accepted 5 October 2014

Keywords:
Neuromusculoskeletal modeling
EMG
Static optimization
Locomotion
Muscle excitation

ABSTRACT

Current electromyography (EMG)-driven musculoskeletal models are used to estimate joint moments measured from an individual's extremities during dynamic movement with varying levels of accuracy. The main benefit is the underlying musculoskeletal dynamics is simulated as a function of realistic, subject-specific, neural-excitation patterns provided by the EMG data. The main disadvantage is surface EMG cannot provide information on deeply located muscles. Furthermore, EMG data may be affected by cross-talk, recording and post-processing artifacts that could adversely influence the EMG's information content. This limits the EMG-driven model's ability to calculate the multi-muscle dynamics and the resulting joint moments about multiple degrees of freedom. We present a hybrid neuromusculoskeletal model that combines calibration, subject-specificity, EMG-driven and static optimization methods together. In this, the joint moment tracking errors are minimized by balancing the information content extracted from the experimental EMG data and from that generated by a static optimization method. Using movement data from five healthy male subjects during walking and running we explored the hybrid model's best configuration to minimally adjust recorded EMGs and predict missing EMGs while attaining the best tracking of joint moments. Minimally adjusted and predicted excitations substantially improved the experimental joint moment tracking accuracy than current EMG-driven models. The ability of the hybrid model to predict missing muscle EMGs was also examined. The proposed hybrid model enables muscle-driven simulations of human movement while enforcing physiological constraints on muscle excitation patterns. This might have important implications for studying pathological movement for which EMG recordings are limited.

1. Introduction

Human movement emerges from synaptic commands generated by central and peripheral neural circuitries, ultimately converging to pools of alpha motor neurons (Farina and Negro, 2012). Muscles innervated by firing motor neurons are recruited and their coordinated activity generates reaction forces throughout the skeletal system and interaction with the environment. The transformations involved are non-linear and neuromusculoskeletal modeling is a promising approach to understand how neural commands are translated into mechanical output by multiple musculotendon units (MTUs) spanning multiple degrees of freedom (DOFs) (Buchanan et al., 2004; Geyer and Herr, 2010; Lloyd and Besier, 2003; Sartori et al., 2012a).

Surface electromyography (EMG) indirectly reflects the neural drive to muscles and is easily recorded during movement. Subsequently, EMG-linear envelopes have been used to drive neuromusculoskeletal models (i.e. EMG-driven modeling) during a variety of dynamic motor tasks and predict resulting joint moments (Besier et al., 2009; Krishnaswamy et al., 2011; Manal et al., 2002; Sartori et al., 2012a). In these, the underlying musculoskeletal model is scaled and calibrated to an individual's anthropometry and EMG-force generating properties. However, calibrated EMG-driven models do not always well predict the experimental moments around multiple DOFs (Sartori et al., 2012a). This is partly due to intrinsic limitations in surface EMG including (1) the inability to access deep muscles, (2) noise contamination from cross-talk and movement artifacts, and (3) the EMG-linear envelope extraction procedure that may not properly demodulate neural excitations from the motor neurons action potentials (Farina and Negro, 2012). Furthermore, EMG-linear

* Correspondence to: Universitaetsmedizin Goettingen, Georg-August-Universitaet, Department of Neurorehabilitation Engineering, Bernstein Focus Neurotechnology Goettingen, Bernstein Center for Computational Neuroscience, Von-Siebold-Str. 3, D – 37075 Goettingen, Germany. Tel.: +49 551 39 20 406; fax: +49 551 39 20 110.
E-mail address: massimo.srt@gmail.com (M. Sartori).

http://dx.doi.org/10.1016/j.jbiomech.2014.10.009
0021-9290/

envelopes are normalized to peak values to reflect percentage excitation levels. This adds uncertainties, as true EMG-maxima are difficult to attain. Therefore, amplitude-normalized EMG-linear envelopes roughly approximate muscle excitations and may limit EMG-driven models' abilities in predicting musculoskeletal dynamics. Therefore, there is a need for modeling methods that can generate EMG-informed simulations of human movement, while accounting for surface EMG limitations.

An alternative to EMG-driven modeling is to use optimization to solve for muscle excitations (Anderson and Pandy, 2001; Erdemir et al., 2007; Seth and Pandy, 2007). However, even though optimization methods can represent EMG-linear envelopes in some instances (Hamner and Delp, 2013; Thelen and Anderson, 2006), it has been shown that, for the same joint moments and angles, different individuals use different excitation patterns depending on the control tasks (Buchanan and Lloyd, 1995; De Serres and Milner, 1991; Tax et al., 1990), pathology (Besier et al., 2009; Fregly et al., 2012; Shao et al., 2009), and training (Menegaldo and Oliveira, 2011; Norton and Gorassini, 2006). Nevertheless, optimization does ensure close tracking of experimental joint dynamics: so can combined EMG-driven and optimization methods be used to overcome limitations of both approaches?.

We present the development of combined EMG-driven modeling (Lloyd and Besier, 2003; Sartori et al., 2012a) with static optimization methods (Anderson and Pandy, 2001; Erdemir et al., 2007). We call this a hybrid EMG-informed neuromusculoskeletal model, or hybrid model. The hybrid model minimizes joint moment tracking errors by balancing the information content extracted from experimental EMG data with that generated by a static optimization method.

We describe and explore the theoretical aspects of this methodology to minimally adjust EMG-linear envelopes, which we now call excitations, and predict muscle excitations for which EMGs are not available, while attaining best tracking of joint moments. We then investigate if the hybrid model can generate excitations reflecting muscle patterns across individuals and motor tasks. We finally assess the hybrid model's ability of estimating missing EMG-excitations.

2. Methods

2.1. Human movement data collection

The Human Research Ethics Committee at the University of Western Australia approved all procedures and all participants provided their informed, written consent. Motion capture data were recorded from five healthy male subjects (age: 26.6 ± 1.3 years, weight: 73.9 ± 11.8 kg, height: 1.77 ± 0.1 m) who performed one static anatomical pose, and eight repeated trials of ground level walking (2.0 ± 0.19 m/s) and running (4.7 ± 0.4 m/s). Dynamic trial recordings included the full stance phase of the subjects' right lower extremity. Each subject had 27 retro-reflective markers placed on the right and left lower extremities as well as on the pelvis and trunk (Dempsey et al., 2009). Three-dimensional marker locations were recorded (250 Hz) using a 12-camera system (Vicon, Oxford Metrics, Oxford, UK). Ground reaction forces (GRFs) and EMG data were recorded (2000 Hz) using an in-ground force plate (AMTI, Watertown, MA) and a 16-channel acquisition system (Noraxon, Scottsdale, USA) respectively. Both GRFs and marker trajectories were low-pass filtered with the same zero-phase fourth-order Butterworth filter. Cut-off frequencies (between 8 and 14 Hz) were determined by trial-specific residual analysis (Winter, 2009). EMGs were collected from 16 muscle groups of the right lower extremity (Table 1) and underwent band-pass filtering (30–450 Hz), full-wave rectification, and low-pass filtering (6 Hz) using a zero-phase second-order Butterworth filter. For each subject and muscle, the resulting linear envelopes were normalized with respect to peak-processed values obtained from the entire set of recorded trials. One dataset was created for the hybrid model calibration and tuning, i.e. two walking and two running trials per subject. Another was created for the hybrid model validation, i.e. six walking and six running trials per subject.

2.2. Movement modeling

We used OpenSim (Delp et al., 2007) to scale a generic whole-body model of the musculoskeletal geometry (Hamner et al., 2010) to match each subject's anthropometry. The musculoskeletal geometry model had 12 segments and 19 DOFs across trunk, pelvis and right/left lower extremities and had 34 MTUs in the right lower extremity (Table 1) as previously described (Sartori et al., 2012a). During the scaling process virtual markers were placed on the generic musculoskeletal geometry model based on the position of the experimental markers from the static poses. The model anthropomorphic properties were then linearly scaled on the basis of the relative distances between experimental and corresponding virtual markers (Delp et al., 2007). The OpenSim inverse kinematics (IK) algorithm solved for joint angles that minimized the least-squared error between experimental and virtual marker locations. The IK-generated kinematics and the experimental GRFs were used to obtain joint moments via inverse dynamics (ID) and

Table 1
Muscle groups from which experimental electromyography (EMG) signals were recorded and the associated musculotendon units (MTUs) that were driven by these EMGs. In this, the gluteus medius EMGs also drove the gluteus minimus MTUs. The vastus intermedius EMG activity was derived as the mean between the vastus lateralis and vastus medialis EMGs (Lloyd and Besier, 2003). The biceps femoris long head and short head were driven by the same EMG signal. The same applied to the semimembranosus and semitendinosus as well as to the peroneus longus, brevis and tertius. The iliacus and psoas MTUs did not receive experimental EMG input.

Experimental muscle EMG	Musculotendon units
Adductor group	adductor magnus (addmag1, addmag2,addmag3)
	adductor longus (addlong)
	adductor brevis (addbrev)
Gracilis	gra
Gluteus maximus	gmax1, gmax2, gmax3
Gluteus medius	gmed1, gmed2, gmed3
	gluteus minimus (gmin1, gmin2, gmin3)
Tensor fasciae latae	tfl
Lateral hamstring	biceps femoris long head (bicfemlh)
	biceps femoris short head (bicfemsh)
Medial hamstring	semimembranosus (semimem)
	semitendinosus (semiten)
Rectus femoris	recfem
Sartorius	sar
Vastus lateralis	vaslat
Vastus medialis	vasmed
(Vastus lateralis+Vastus medialis)/2	vastus intermedius (vasint)
Gastrocnemius lateralis	gaslat
Gastrocnemius medialis	gaslat
Soleus	sol
Peroneus group	peroneus longus (perlong)
	peroneus brevis (perbrev)
	peroneus tertius (pertert)
Tibialis anterior	tibant

residual reduction analysis (RRA) (Thelen and Anderson, 2006). We call these the "experimental joint moments". The alternative pathway was by the hybrid model.

2.3. Hybrid model

The hybrid model (Fig. 1) combines a calibrated, forward dynamic, *EMG-driven model* of the right lower extremity (Lloyd and Besier, 2003; Buchanan et al., 2004; Winby et al., 2008; Sartori et al., 2012a), with a tuned *static optimization component* (Anderson and Pandy, 2001; Crowninshield and Brand, 1981; Erdemir et al., 2007). Parameters and coefficients in these two components were identified in a two-step procedure. The first step was the *calibration* of the EMG-driven model's parameters. The second was the *tuning* of the static optimization coefficients. These two steps only used data from the calibration/tuning trials (Section 2.1). The calibrated/tuned hybrid model was then evaluated using data from the validation trials (Section 2.1). During calibration/tuning and validation the hybrid model simulated the stance phase of the subjects' right lower extremity for walking and running. In the following of this section we describe the hybrid model's two components and their respective identification steps.

The *EMG-driven model* component (Fig. 1) used four segments, five DOFs, and 34 MTUs (i.e. as defined in Fig. 1 and Table 1) of the right lower extremity from the whole-body, subject-specific, OpenSim model used for the IK, ID and RRA analyses (Section 2.2). This component was based on our previously presented EMG-driven model (Sartori et al., 2012a) and comprised four main blocks. The MTU kinematics block received IK-generated DOF-angles and computed MTU kinematic, i.e. length and moment arms using one B-spline function per MTU (Sartori et al., 2012b). MTU-specific splines were created using MTU length nominal data from the scaled OpenSim model (Sartori et al., 2012b). The EMG-to-activation dynamics block received 16 EMG-excitations and redistributed them to 32 MTUs as described in Table 1 and in our previous work (Sartori et al., 2012a). This block also received iliacus and psoas excitations generated by the static optimization component (see below) because these MTUs had no experimental EMG data available. Initial excitations were processed using a time-history dependent recursive filter and a non-linear transfer function to account for the non-linear excitation–force relationship and determine the resulting activation (Buchanan et al., 2004). The previously presented MTU contraction dynamics block (Buchanan et al., 2004; Lloyd and Besier, 2003) used a Hill-type muscle model to estimate MTU forces from MTU lengths and activations estimated in the previous blocks. Joint moments were computed as the product of each MTU force and their associated moment arms computed in previous blocks. The calibration of the EMG-driven model was performed to obtain the best predictions of the experimental joint moments when only driven by the experimental EMG-excitations and joint angles from the calibration trials (Buchanan et al., 2004; Lloyd and Besier, 2003; Sartori et al., 2012a). Calibration identified parameters that varied non-linearly with subjects' anthropometry including EMG-to-activation filtering and non-linearity coefficients, and MTU optimal fiber length, tendon slack length, and maximal isometric force. Simulated annealing (Goffe et al., 1994) varied these parameters within pre-defined boundaries to minimize the cumulative sum of the root mean square error (RMSE) between predicted and experimental joint moments about all DOFs and calibration trials simultaneously.

The *static optimization* component (Fig. 1) predicted iliacus and psoas excitations and adjusted the initial EMG-excitations for the remaining 32 MTUs (Table 1). Adjusted and predicted excitations were found that simultaneously minimized three terms: (1) $E_{trackMOM}$, i.e. sum of squared differences between predicted and experimental joint moments; (2) $E_{trackEMG}$, i.e. sum of absolute differences between adjusted and experimental EMG-excitations for the 32 MTUs with EMG data available (Table 1), and (3) E_{sumEXC}, i.e. sum of squared excitations for all 34 MTUs. These were combined in the following objective function, which was minimized frame-by-frame using simulated annealing (Goffe et al., 1994):

$$F_{obj} = \alpha E_{trackMOM} + \beta E_{sumEXC} + \gamma E_{trackEMG}, \quad (1)$$

where (α,β,γ) are positive weighting coefficients. Tuning of the static optimization component coefficients was performed to obtain the best balance in tracking both the experimental excitations and joint moments. The minimization of Eq. (1) depends on the relative values of (α,β,γ). A coefficient that is larger than the others would result in the corresponding error term undergoing greater minimization compared to the other terms. To-this-end, α was arbitrarily assigned the value of 1 and the corresponding relative (β,γ) values were tuned to ensure equally low ($E_{trackEMG}$, $E_{trackMOM}$). The $E_{trackMOM}$–$E_{trackEMG}$ relationship was experimentally analyzed by varying $0 \le \beta \le 300$ (in 30 steps), and $0 \le \gamma \le 3000$ (in 60 steps) with $\alpha = 1$. The $\beta = 300$ upper-bound was experimentally found so that $E_{trackMOM} \le E^{EMG}_{trackMOM}$ across all calibration trials and subjects, with $E^{EMG}_{trackMOM}$ being the largest joint moment tracking error, i.e. from the calibrated, EMG-driven model that used experimental EMG-excitations. The $\gamma = 3000$ upper-bound was experimentally found so that $E_{trackEMG} \le 10^{-3}$ for all calibration trials and subjects, with 10^{-3} representing the threshold beyond which discrepancies between predicted and experimental excitations were assumed to be negligible. By varying (β,γ), the hybrid model produced 30×60 values for ($E_{trackMOM}$, $E_{trackEMG}$, E_{sumEXC}), for each calibration trial and subject. For each subject and motor task, these terms were normalized to their highest value and averaged across all respective calibration trials. This resulted in subject-specific and motor task-specific terms, i.e. ($\hat{E}_{trackMOM}$, $\hat{E}_{trackEMG}$, $\hat{E}_{sumEXC}$).

With β held constant and γ being varied across the 60 steps, the corresponding $\hat{E}_{trackMOM}$-values were plotted versus the associated $\hat{E}_{trackEMG}$-values. Our experimental results showed that, for a given β-value, the $\hat{E}_{trackMOM}$–$\hat{E}_{trackEMG}$ relationship was always represented by an L-shaped curve (Fig. 2). L-shaped curves were therefore generated for the 30 β-values. For each $\hat{E}_{trackEMG}$-value, the point associated to the lowest $\hat{E}_{trackMOM}$ was chosen to produce the "best" $\hat{E}_{trackMOM}$–$\hat{E}_{trackEMG}$ curve (Fig. 2). The "knee-point" of the best $\hat{E}_{trackMOM}$–$\hat{E}_{trackEMG}$ curve represented the minimum level of EMG-adjustment resulting in the maximum improvement in experimental joint moment tracking accuracy. The "knee-point" was found by applying the L-method (Salvador and Chan, 2005), which identified the point of intersection of two piecewise regression lines that best fit the L-shaped $\hat{E}_{trackMOM}$–$\hat{E}_{trackEMG}$ curve. In some cases multiple L-curves associated with different $\hat{E}_{sumEXC}$-values (or β-values) could pass through the same "knee-point" (Fig. 2). In these cases, the curve associated to the lowest $\hat{E}_{sumEXC}$-value was chosen and the

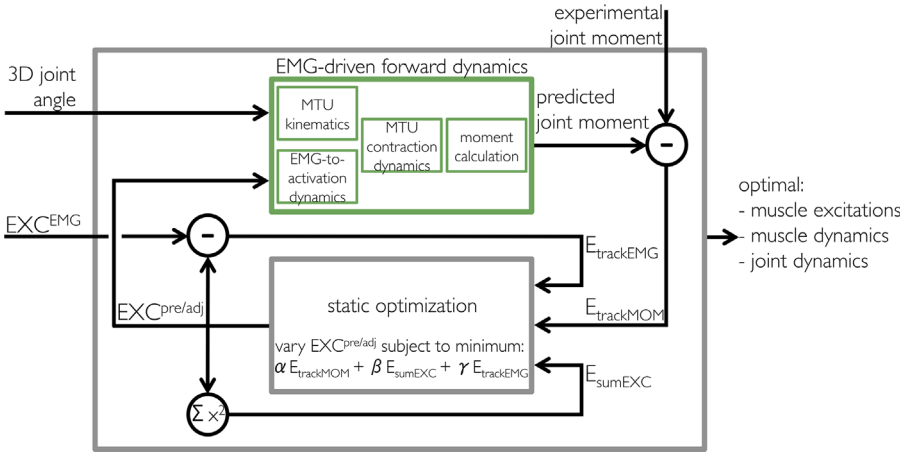

Fig. 1. Schematic representation of the hybrid model. The algorithm is applied at each time step of the simulation. The hybrid model comprises of two main components: the EMG-driven forward dynamics model, and the static optimization component. The EMG-driven model is based on a four-segment, five-DOF, 34-MTU human lower extremity model (Sartori et al., 2012a). Segments include the pelvis, thigh, shank, and foot from the subject-specific OpenSim model used for inverse kinematics and dynamics analyses (Section 2.2). DOFs include: hip flexion–extension, hip adduction–abduction, hip internal–external rotation, knee flexion–extension, and ankle plantar–dorsi flexion. MTUs are listed and defined in Table 1 (Sartori et al., 2012a). The EMG-driven model is initially calibrated using experimental EMG-excitations (EXC^{EMG}), experimental three-dimensional (3D) joint angles, and matching experimental joint moments from a set of calibration trials. The static optimization component minimally adjusts experimental excitations (EXC^{adj}) and predicts excitations for those MTUs without experimental EMGs available (EXC^{pre}). In this, the α, β and γ coefficients as well as the joint moment tracking error ($E_{trackMOM}$), EMG tracking error ($E_{trackEMG}$) and sum of squared excitations (E_{sumEMG}) terms in the objective function (i.e. Eq. (1)) are determined using the methods in Section 2.3. The hybrid model generates predicted and minimally adjusted excitation for 34 MTUs ($EXC^{pre/adj}$) and predicts resulting joint moments about the five DOFs.

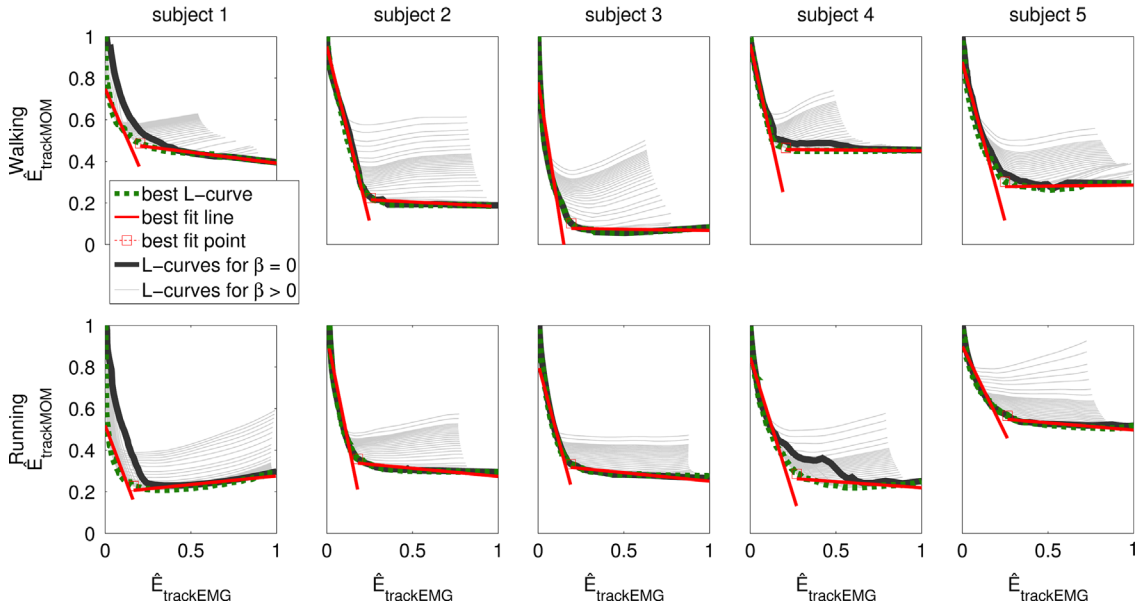

Fig. 2. L-shaped relationships between EMG-excitation tracking errors ($\hat{E}_{trackEMG}$) and experimental joint moment tracking errors ($\hat{E}_{trackMOM}$) during walking (top row) and running (bottom row). Thick black lines and thin gray lines represent the L-curves for values of $\beta=0$ and $\beta>0$ respectively (Eq. (1), Section 2.3). The dashed green line represents the best L-curve (Section 2.3) used to determine the "knee" point (i.e. best fit point) and the final values of β and γ in Eq. (1) (Table 1). Graphs represent curves averaged across the calibration trial dataset of each subject (Section 2).

Table 2
The α, β and γ coefficients for the hybrid model objective function (Eq. (1), Fig. 1) and the associated best-fit ($\hat{E}_{trackMOM}$, $\hat{E}_{trackEMG}$) "knee" point coordinates (Fig. 2).

	Subject 1	Subject 2	Subject 3	Subject 4	Subject 5
Walking					
α	1	1	1	1	1
β	7.5	7.5	0.2	15	7.5
γ	15	10	5	15	15
$\hat{E}_{trackEMG}$	0.20	0.26	0.19	0.21	0.25
$\hat{E}_{trackMOM}$	0.49	0.22	0.10	0.46	0.30
Running					
α	1	1	1	1	1
β	45	0.2	10	20	5
γ	65	30	30	25	40
$\hat{E}_{trackEMG}$	0.17	0.18	0.19	0.27	0.26
$\hat{E}_{trackMOM}$	0.23	0.36	0.33	0.29	0.57

corresponding β-value was selected. Low $\hat{E}_{sumEXC}$-values (i.e. high β values) ensured excitation peaks were distributed across all MTUs and prevented them from saturating. The corresponding γ coefficient producing the $\hat{E}_{trackEMG}$-value at the "knee-point" was then chosen. This process generated subject-specific, motor task-specific (β,γ)-values.

3. Validation procedures

The first test assessed the hybrid model's ability to simultaneously (1) adjust EMG-excitations minimally, (2) predict deeply located iliacus and psoas excitations, while (3) improving the joint moment prediction accuracy. The second test quantified the hybrid model's ability to predict missing muscle excitations. To-this-end, the muscle groups' EMG-excitations were omitted one by one before the calibration step. The calibrated hybrid model was then used to predict excitations of the omitted muscles. This calibration–validation process was repeated for all 16 muscles (Table 1).

Model estimates were time-normalized to 100 samples using cubic splines. Experimental and predicted joint moments were normalized to subject's mass. Similarity between predicted and experimental quantities (i.e. joint moments and muscle group/MTU excitations) was calculated using the Pearson product moment correlation coefficient R as well as R^2 and the RMSE.

We performed a one-way repeated-measures ANOVA to compare similarity coefficients variation over the validation trials across the five subjects for a given MTU/DOF. We performed a Kolmogorov–Smirnov test (significance level = 0.05) to ensure data were normally distributed before performing the ANOVA. Differences across subjects were considered significant with $p<0.01$.

4. Results

The "knee-points" derived from the $\hat{E}_{trackMOM}$–$\hat{E}_{trackEMG}$ curves resulted in similar levels of EMG-adjustment across subjects and tasks. The knee-point's $\hat{E}_{trackEMG}$ coordinate was 0.22 ± 0.03 during walking and 0.21 ± 0.04 during running trials, across subjects (Table 2). In these, 0 and 1 respectively represent no and maximum adjustment of experimental excitations. The knee-point's $\hat{E}_{trackMOM}$ coordinate ranged from 0.10 ± 0.04 (Subject3) to 0.49 ± 0.05 (Subject1) during walking trials and from 0.23 ± 0.04 (Subject1) to 0.57 ± 0.05 (Subject5) during running trials. In these, 0 represents full experimental joint moment matching and 1 represents the maximum allowed joint moment tracking error $E^{EMG}_{trackMOM}$ (Section 2.3).

For the validation dataset, experimental and minimally adjusted excitations displayed substantial similarities. For walking (Fig. 3) there were no statistical differences across subjects and trials in the RMSEs and R^2 for 10 MTUs including: addmag3, gmax1-2, gmin1, gmin3, sol, tibant, vasint, vaslat, and vasmed. For these, RMSEs were always ≤ 0.09 and R^2 always ≥ 0.73. The remaining 22 MTUs (Fig. 3) underwent larger excitation adjustments with RMSEs and R^2 statistically varying across subjects. Nevertheless, their RMSEs were always ≤ 0.48 (semiten, Subject3) and R^2 always ≥ 0.15 (recfem, Subject4). For running (Fig. 4), no statistical differences in the RMSEs and R^2 were observed for 14 MTUs including addmag2–3, bicfemlh, gasmed, gmin1-3, gra, recfem, sar, semimem, sol, tibant, and vaslat. Their RMSEs were always ≤ 0.15 and R^2 always ≥ 0.67. The remaining 18 MTUs (Fig. 4) underwent larger excitation adjustments with RMSEs

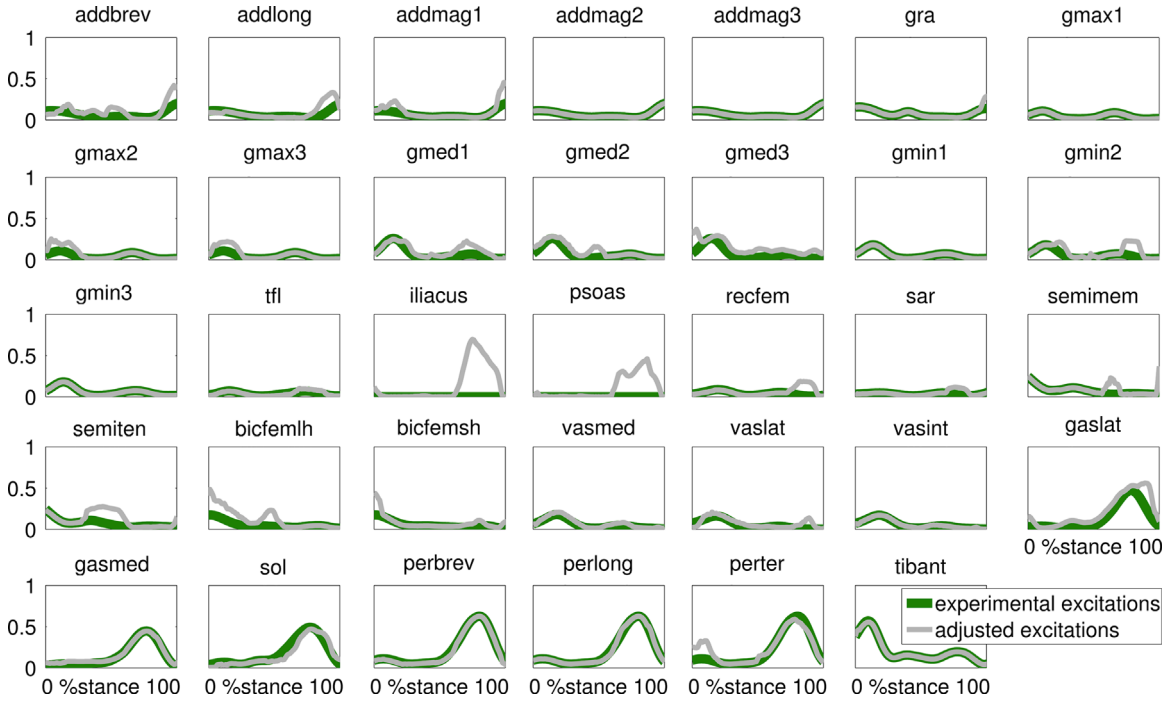

Fig. 3. Experimental, minimally adjusted, and predicted excitations for the 34 musculotendon units (MTU) in the model during walking. Data are averaged across all validation trials and subjects. The MTU names are defined as in Table 1. The reported data are from the stance phase with 0% being heel-strike and 100% toe-off events.

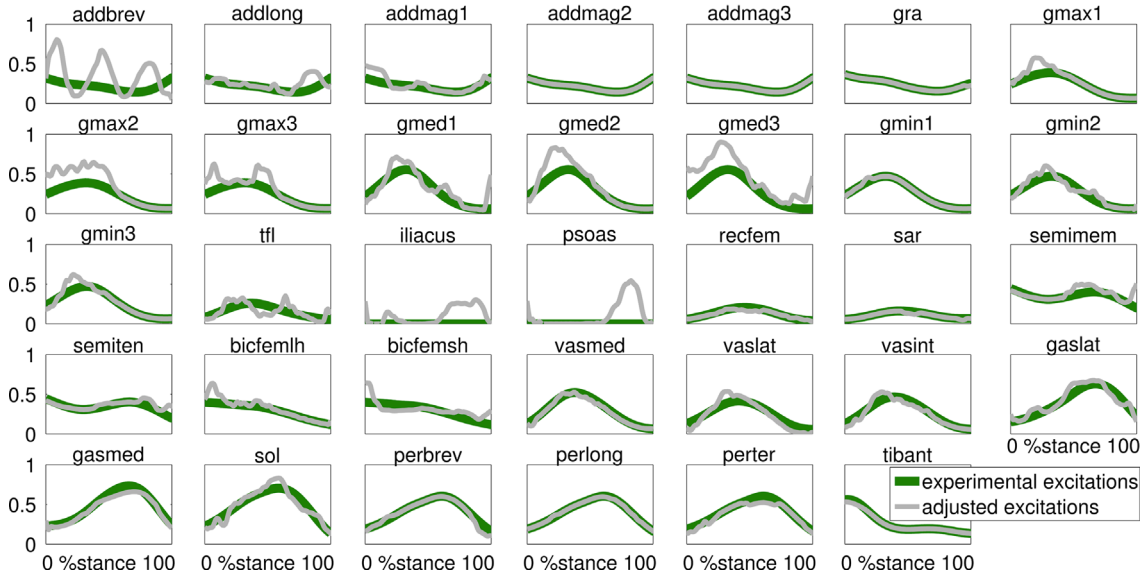

Fig. 4. Experimental, minimally adjusted, and predicted excitations for the 34 musculotendon units (MTU) in the model during running. Data are averaged across all validation trials and subjects. The MTU names are defined as in Table 1. The reported data are from the stance phase with 0% being heel-strike and 100% toe-off events.

and R^2 statistically varying across subjects. Nevertheless, RMSEs were always ≤ 0.49 (addbrev, Subject3) and R^2 always ≥ 0.29 (tfl, Subject1).

Minimally adjusted and predicted excitations resulted in joint moment estimates that matched the experimental moments substantially better than estimates from experimental EMG-excitations as an input to the calibrated EMG-driven model (Fig. 5). The only DOF that did not display substantial improvement in predicted moments was the hip internal–external rotation. During walking and running, there were no statistical differences across subjects and trials in RMSEs and R^2 between experimental and predicted joint moments (Fig. 5; Table 3).

The predicted excitation patterns for the 16 muscles that were sequentially removed from the model showed some level of similarity to their corresponding EMG-excitations (Figs. 6 and 7). The similarity in the excitation amplitude (i.e. RMSEs) was more consistent than that in shape (i.e. R). Across all muscles, trials, and subjects, R largely varied between 0 and 1 and was above 0.5 in 41% of all cases (Fig. 8). The RMSEs between predicted and experimental excitations were consistently below 0.2 in 65% of all cases (Fig. 8).

5. Discussion

We developed a hybrid EMG-informed neuromusculoskeletal model that overcomes limitations in current EMG-driven modeling (e.g. Lloyd and Besier, 2003; Sartori et al., 2012a) and optimization-

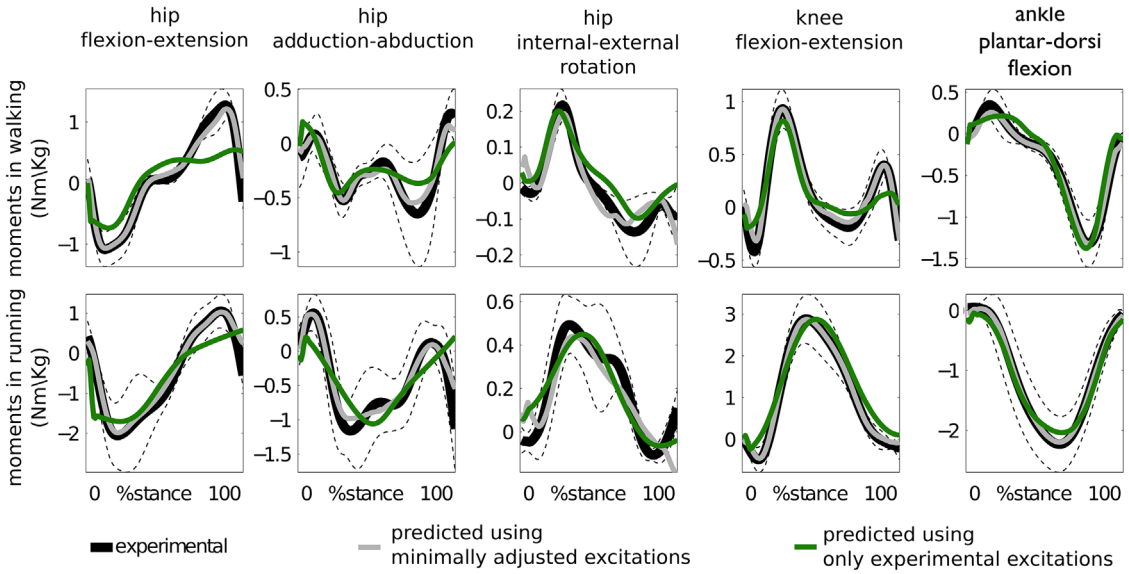

Fig. 5. Joint moments, normalized with respect to body weight, during walking (top row) and running (bottom row) averaged across all validation trials and subjects. The reported joint moments are the experimental, those predicted using minimally adjusted excitations, and those predicted using only experimental excitations (i.e. EMG-linear envelopes). The reported data are from the stance phase with 0% being heel-strike and 100% toe-off events.

Table 3
The RMSE and R^2 coefficients between experimental joint moments and those predicted using either experimental excitations or minimally adjusted excitations. Bold text indicates significant improvement in RMSE and R^2 from using minimally adjusted excitations across individuals with respect to RMSE and R^2 values obtained from using experimental excitations (Sections 3 and 4).

Degree of freedom	Using experimental excitations		Using minimally adjusted excitations		
	RMSE (Nm/kg)	R^2	RMSE (Nm/kg)	R^2	
Hip flexion–extension	0.43 ± 0.13	0.72 ± 0.09	**0.09 ± 0.08**	**0.98 ± 0.02**	Walking
Hip adduction–abduction	0.20 ± 0.15	0.66 ± 0.14	**0.07 ± 0.06**	**0.95 ± 0.07**	
Hip internal–external rotation	0.06 ± 0.02	0.83 ± 0.08	0.04 ± 0.02	0.81 ± 0.10	
Knee flexion–extension	0.18 ± 0.05	0.82 ± 0.07	**0.05 ± 0.04**	**0.97 ± 0.05**	
Ankle plantar–dorsi flexion	0.21 ± 0.05	0.89 ± 0.05	**0.05 ± 0.03**	**0.99 ± 0.01**	
Hip flexion–extension	0.57 ± 0.11	0.74 ± 0.19	**0.19 ± 0.14**	**0.96 ± 0.07**	Running
Hip adduction–abduction	0.44 ± 0.11	0.49 ± 0.19	**0.16 ± 0.07**	**0.93 ± 0.04**	
Hip internal–external rotation	0.13 ± 0.03	0.70 ± 0.21	0.12 ± 0.03	0.71 ± 0.20	
Knee flexion–extension	0.50 ± 0.17	0.89 ± 0.06	**0.07 ± 0.06**	**0.99 ± 0.01**	
Ankle plantar–dorsi flexion	0.24 ± 0.09	0.95 ± 0.03	**0.05 ± 0.03**	**0.99 ± 0.002**	

based approaches (e.g. Anderson and Pandy, 2001; Thelen et al., 2003), while preserving benefits of both methods. Current EMG-driven models take into account realistic subject-specific neuromuscular strategies. However, the predicted musculoskeletal dynamics may be affected by EMG uncertainties resulting from movement, cross-talk, and signal processing artifacts. Furthermore, EMG-driven models are limited to muscles for which EMGs are accessible and available. Alternatively, optimization-based approaches can generate dynamically consistent simulations. However, the underlying neuromuscular redundancy is resolved by using mathematical constraints and assumptions, which do not necessarily generalize across individuals, motor tasks, and orthopedics/neurological conditions (Buchanan and Lloyd, 1995; Menegaldo and Oliveira, 2011; Shao et al., 2009; Tax et al., 1990).

The hybrid model generated musculoskeletal simulations that were consistent both with experimental electrophysiological data and joint dynamics (Fig. 2). Across all individuals and motor tasks, the hybrid model tracked experimental joint moments (Fig. 5) by minimally adjusting experimental excitations and predicting MTU excitations for which EMGs were not available (Figs. 3 and 4). Furthermore, the hybrid model used EMG-calibrated MTU-parameters that reflected subject-specific EMG-force relationships. Current optimization-based approaches do not rely on EMG-calibrated parameters and have therefore limited capabilities in using EMGs to directly inform the underlying musculoskeletal model.

Our results also confirmed that static optimization-based methods alone can only capture some of the trends in the experimental EMGs across walking and running as previously reported (Hamner and Delp, 2013; Liu et al., 2008). Muscle excitations generated by the hybrid model's static optimization component (i.e. no EMG tracking) displayed similarity with corresponding EMGs that better matched amplitude (RMSE) than shape (R) (Figs. 6–8). In five muscles, predicted and experimental excitations had little agreement in both amplitude and shape, i.e. RMSEs > 0.1 and $R < 0.5$ in more than 60% of all cases. These included gracilis, sartorius, vastus medialis, gastrocnemious medialis, and peroneus group. For these, it is recommended to record EMG data to use for tracking during the hybrid model-based simulations. However, both gracilis and sartorius have the smallest physiological cross-sectional areas among the hip and knee muscles (Sartori et al., 2012a). Therefore, imprecision in their predicted excitations may have limited consequences in the joint moment prediction accuracy. Future work could use bases of excitation primitives to constrain the solution space of the hybrid model's static optimization component and possibly generate more physiologically-consistent excitations for muscles with no EMGs available (Allen and Neptune 2012; De Groote et al., 2012; Sartori et al., 2013; Walter et al., 2014).

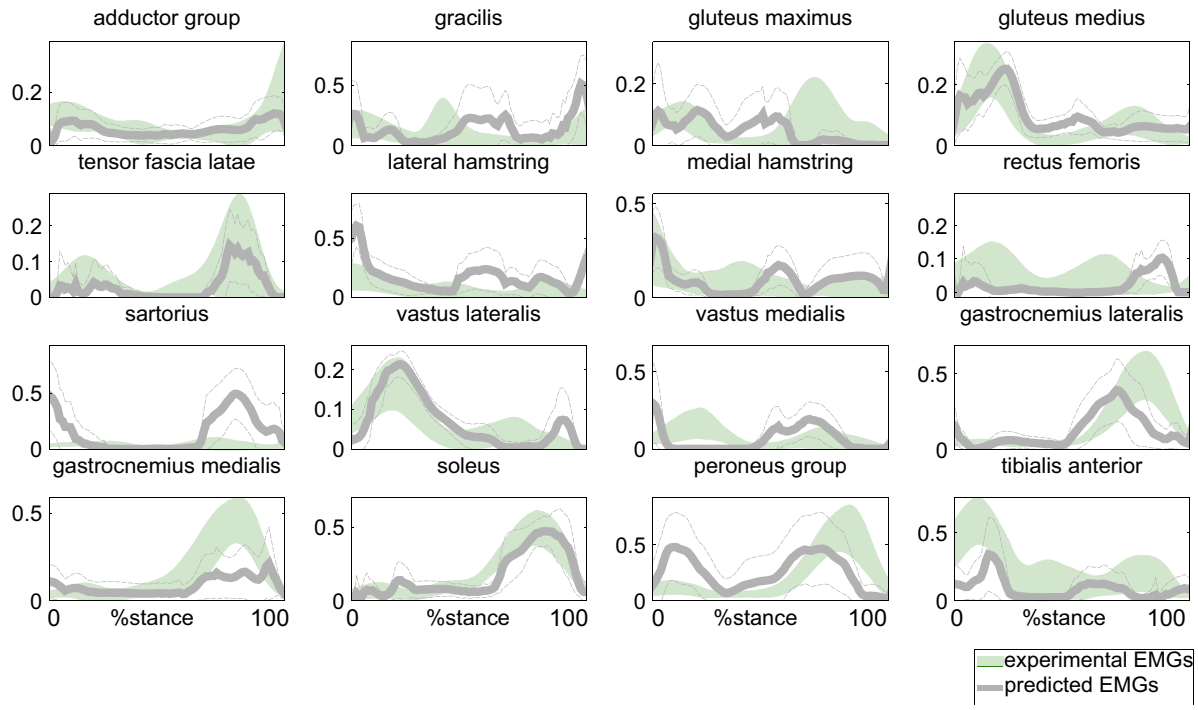

Fig. 6. The average experimental EMG-linear envelopes (green area representing ± 1 standard deviation) and matching predicted EMGs (solid gray line; dashed lines represents ± 1 standard deviation) during walking. Data are shown for the 16 muscle groups from which EMGs were recorded. Data are averaged across all validation trials and subjects and are reported for the stance phase with 0% being heel-strike and 100% toe-off events.

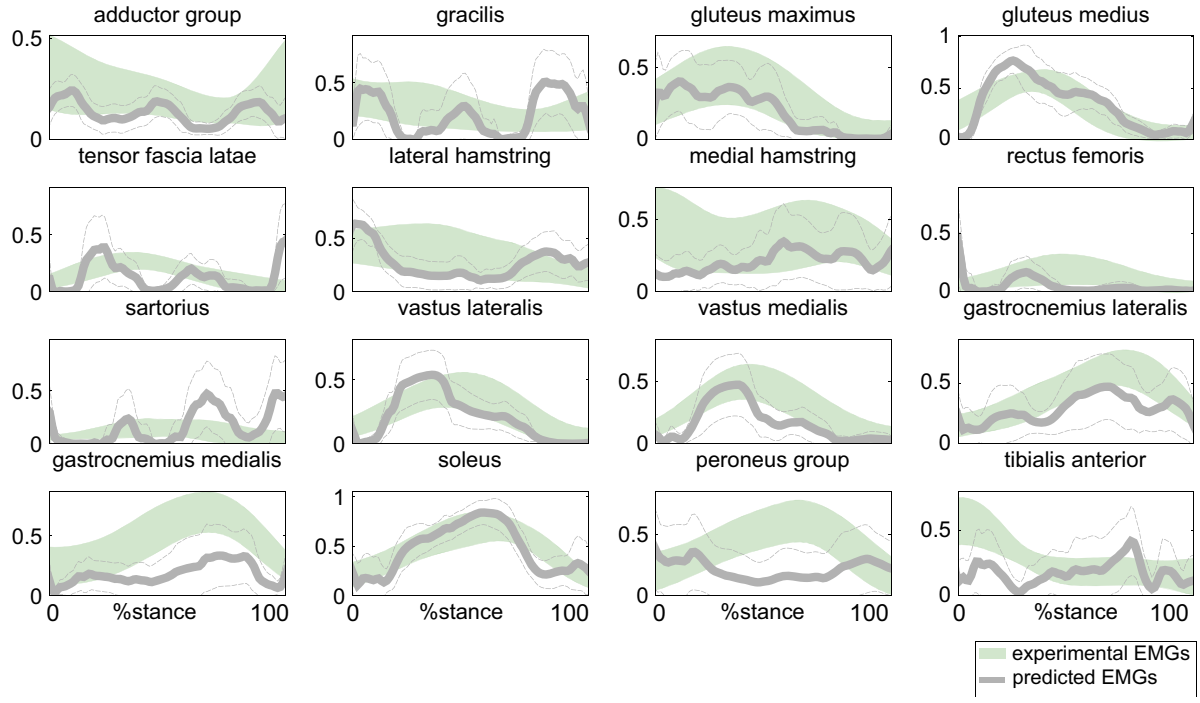

Fig. 7. The average EMG-linear envelopes (green area representing ± 1 standard deviation) and matching predicted EMGs (solid gray line; dashed lines represents ± 1 standard deviation) during running. Data are shown for the 16 muscle groups from which EMGs were recorded. Data are averaged across all validation trials and subjects and are reported for the stance phase with 0% being heel-strike and 100% toe-off events.

However, the hybrid model's ability of mixing excitations from EMGs and static optimization allows taking into account subject-specific neuromuscular strategies and how they vary across conditions. This is especially important for translating musculoskeletal modeling to the patient level. In this regard, current optimization-based methods would have limited capacity in capturing non-physiological muscular behavior by means of an arbitrary objective function (Higginson et al., 2012) or basis of excitation primitives (De Groote et al., 2012). In the context of our method, experimental EMGs could be recorded for target muscles that reflect the patient's

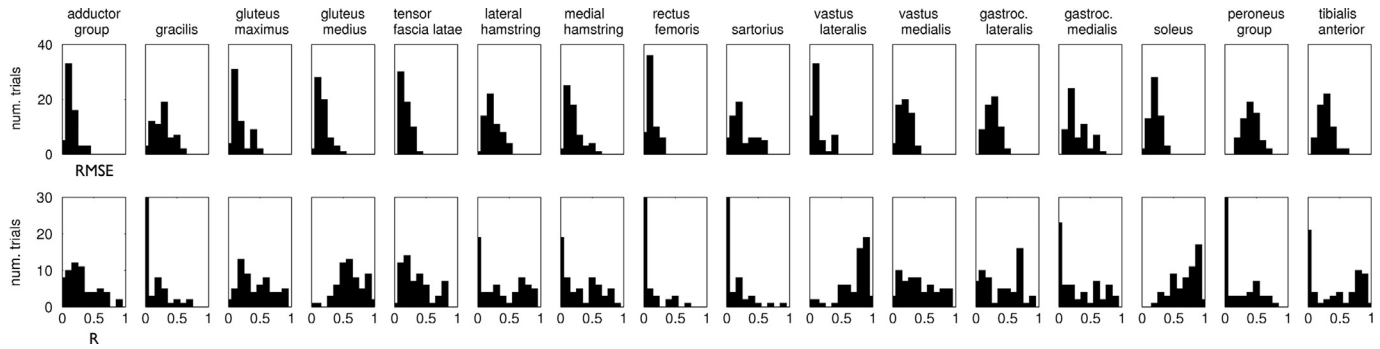

Fig. 8. The distribution of the correlation coefficient (R) and the root mean squared error (RMSEs) between experimental and predicted excitations for the 16 muscle groups that were sequentially removed from the EMG-driven model calibration procedure (Table 1, Figs 6 and 7). The histograms report RMSE (top row) and R (bottom row) distributions across all validation trials performed by all subjects (i.e. 60 validation trials per muscle in total). In each graph, the x-axis reports the full range of observed RMSE and R values, i.e. $0 \leq \text{RMSE}$, $R \leq 1$. The y-axis reports the number of trials that fell in a specific RMSE- or R-interval.

non-physiological muscular behavior. These could be used to calibrate/tune the hybrid model and generate EMG-informed simulations that track patient-specific muscle recruitment strategies and joint dynamics, while underling patient-specific EMG-force relationships.

The case study in Higginson et al. (2012) outlined preliminary results and benefits from a hybrid simulation generated using computed muscle control (CMC) (Thelen et al., 2003) for one post-stroke patient. EMG-driven modeling (Shao et al., 2009) was used to identify patient-specific parameters and predict activations in four ankle muscles. These were used to constrain CMC-generated activations. However, results had limited generalizability as they were from one gait cycle only. Furthermore, CMC-predicted activations were constrained to EMG-activations using manual tuning.

Our approach provided an analytical method for identifying the (α,β,γ)-coefficients that ensured best balance between EMG and joint moment tracking errors (Fig. 2), thus avoiding manual tuning. This resulted in minimal and repeatable levels of EMG-adjustment ($\hat{E}_{trackEMG}=0.22\pm0.03$ during walking and 0.21 ± 0.04 during running). The variability in the underlying (α,β,γ)-coefficients (Table 2) might reflect sensitivity to the initial EMG-driven model calibration and EMG normalization procedures. These procedures influence the model's capability of predicting joint moments and the EMG-adjustments required across individuals. Future work will explore whether improved model calibration and EMG-amplitude estimation procedures can result in more consistent coefficients across individuals and motor tasks (Clancy et al., 2006, 2001).

The sharp drop in joint moment tracking error (Fig. 2) that resulted from allowing a minimal EMG-adjustment (Figs. 3 and 4) suggests that joint dynamics was explained by neuromuscular solutions that were close to the initial EMG data. The model-based EMG-minimal adjustment may give insights into neural drive modulations that might have been filtered out and/or contaminated by surface EMG artifacts (Clancy et al., 2006; Farina and Negro, 2012). Future research will also investigate the hybrid model's ability at decreasing EMG cross-talk by exploiting the proposed minimal adjustment criterion.

Some limitations of this study should be recognized. The hybrid model was not used to compute segmental/joint kinematics. This was done to reduce the computational demand of numerical integration, which if used would have substantially slowed the calibration and tuning procedures. However, we used OpenSim's RRA to ensure dynamic consistency between tracked joint moments and experimental joint kinematics. Therefore, the minimally adjusted and predicted excitations also reflected the observed kinematics. Additionally, we have shown that calibrated EMG-driven models can predict joint kinematics using full forward dynamics models (Barrett et al., 2007). Future work will therefore couple the hybrid method with full-forward dynamic models and postural controllers (Latash, 2010; Leroux et al., 2002; Wang et al., 2007). This will enable calibrated and tuned full-forward dynamics simulations informed by minimally adjusted excitations with reduced computational requirements.

Results were generated during stance phases only, because calibration included running trials for which the swing phase occurred out of the motion capture volume. Therefore, there was an incomplete swing phase data available for calibration/validation across trials.

The hybrid model was validated on novel trials that were, however, of the same type than the trials used for calibration/tuning. Nevertheless, all trials were performed at self-selected speeds. As a result, validation trials underlay locomotion speeds that differed from those observed across calibration/tuning trials (Supplementary Fig. 1). Therefore, validation provided initial evidence of the model's extrapolation ability under novel speed conditions. However, the hybrid model is ultimately a tracking method. It enables musculoskeletal simulations that track experimental joint moments for any novel task and condition, whether or not these were used for calibration/tuning. Nevertheless, calibration/tuning enable tracking experimental joint moments with smaller adjustments in the EMG-excitations than using a non-calibrated/non-tuned model. Understanding which motor tasks and which facets of the motors tasks are best for calibrating/tuning, and how the resulting hybrid model tracks the experimental data outside the range of calibration/tuning trials is an important question that requires a structured research, which was beyond the scope of this work.

The hybrid model could be employed to possibly generate improved predictions of knee joint contact forces compared to current EMG-driven approaches (Gerus et al., 2013; Manal and Buchanan, 2013; Kumar et al., 2012; Walter et al., 2014). Furthermore, estimation of hip joint contact forces can currently only be done using optimization-based techniques (Modenese and Phillips, 2011). The hybrid approach could be employed as it estimates excitations for deep hip muscles and adjusts the excitations of superficial hip muscles with multiple compartments (Fernandez et al., 2014). The hybrid model's ability of tracking EMGs and joint moments for each time-point can enable real-time applications. The model could be applied to develop control systems for functional electrical stimulation (FES) interventions or wearable exoskeletons. Adjusted excitations could be used to generate instantaneous control commands for the assistive device (i.e. FES or exoskeleton system), which will provide minimal and optimal support to the impaired individual throughout a selected task. All these possibilities require further research.

The primary value of the hybrid model is that it combines EMG-driven modeling with the added benefits of optimization-based approaches, and provides fully automated methods for calibration/tuning that well track both experimental joint moments and

EMG-excitations. This opens up avenues for examining human neuromuscular control and biomechanics in healthy and pathological individuals with applications in advanced neurorehabilitation treatments and technologies.

Conflict of interest statement

There are no known conflicts of interest associated with this publication and there has been no significant financial support for this work that could have influenced its outcome.

Acknowledgments

The hybrid model was developed as part of the Calibrated EMG-Informed Neuromusculoskeletal Modeling Toolbox (CEINMS, https://simtk.org/home/ceinms). We would like to thank Dr. Monica Reggiani and Claudio Pizzolato for optimizing the final code for speed and modularity. This work was supported by the European Research Council (ERC), Belgium via the ERC Advanced Grant DEMOVE [267888], and in part by the National Institutes of Health (NIH), United States [Grant-RO1-EB009351] and the National Health and Medical Research Council, Australia [628850].

Appendix A. Supplementary materials

Supplementary materials associated with this article can be found in the online version at http://dx.doi.org/10.1016/j.jbiomech.2014.10.009.

References

Allen, J.L., Neptune, R.R., 2012. Three-dimensional modular control of human walking. J. Biomech. 45, 2157–2163.
Anderson, F.C., Pandy, M.G., 2001. Static and dynamic optimization solutions for gait are practically equivalent. J. Biomech. 34, 153–161.
Barrett, R., Besier, T., Lloyd, D., 2007. Individual muscle contributions to the swing phase of gait: an EMG-based forward dynamics modeling approach. Simul. Model. Pract. Theory 15, 1146–1155.
Besier, T.F., Fredericson, M., Gold, G.E., Beaupré, G.S., Delp, S.L., 2009. Knee muscle forces during walking and running in patellofemoral pain patients and pain-free controls. J. Biomech. 42, 898–905.
Buchanan, T.S., Lloyd, D.G., 1995. Muscle activity is different for humans performing static tasks which require force control and position control. Neurosci. Lett. 194, 61–64.
Buchanan, T.S., Lloyd, D.G., Manal, K., Besier, T.F., 2004. Neuromusculoskeletal modeling: estimation of muscle forces and joint moments and movements from measurements of neural command. J. Appl. Biomech. 20, 367–395.
Clancy, E.A., Bida, O., Rancourt, D., 2006. Influence of advanced electromyogram (EMG) amplitude processors on EMG-to-torque estimation during constant-posture, force-varying contractions. J. Biomech. 39, 2690–2698.
Clancy, E.A., Bouchard, S., Rancourt, D., 2001. Estimation and application of EMG amplitude during dynamic contractions. IEEE Eng. Med. Biol. Mag. 20 (6), 47–54.
Crowninshield, R.D., Brand, R.A., 1981. A physiologically based criterion of muscle force prediction in locomotion. J. Biomech. 14, 793–801.
De Groote, F., Demeulenaere, B., Swevers, J., De Schutter, J., Jonkers, I., 2012. A physiology-based inverse dynamic analysis of human gait using sequential convex programming: a comparative study. Comput. Methods Biomech. Biomed. Eng. 15, 1093–1102.
De Serres, S.J., Milner, T.E., 1991. Wrist muscle activation patterns and stiffness associated with stable and unstable mechanical loads. Exp. Brain Res. 86, 451–458.
Delp, S.L., Anderson, F.C., Arnold, A.S., Loan, P., Habib, A., John, C.T., Guendelman, E., Thelen, D.G., 2007. OpenSim: open-source software to create and analyze dynamic simulations of movement. IEEE Trans. Biomed. Eng. 54, 1940–1950.
Dempsey, A.R., Lloyd, D.G., Elliott, B.C., Steele, J.R., Munro, B.J., 2009. Changing sidestep cutting technique reduces knee valgus loading. Am. J. Sports Med. 37, 2194–2200.
Erdemir, A., McLean, S., Herzog, W., van den Bogert, A.J., 2007. Model-based estimation of muscle forces exerted during movements. Clin. Biomech. 22, 131–154.
Farina, D., Negro, F., 2012. Accessing the neural drive to muscle and translation to neurorehabilitation technologies. IEEE Rev. Biomed. Eng. 5, 3–14.
Fernandez, J.M., Sartori, M., Lloyd, D.G., Munro, J., Shim, V.B., 2014. Bone remodelling in the natural acetabulum is influenced by muscle force-induced bone stress. Int. J. Num. Method. Biomed. Eng. 30 (1), 28–41.
Fregly, B.J., Boninger, M.L., Reinkensmeyer, D.J., 2012. Personalized neuromusculoskeletal modeling to improve treatment of mobility impairments: a perspective from European research sites. J. Neuroeng. Rehabil. 9, 1–11.
Gerus, P., Sartori, M., Besier, T.F., Fregly, B.J., Delp, S.L., Banks, S.A., Pandy, M.G., D'Lima, D.D., Lloyd, D.G., 2013. Subject-specific knee joint geometry improves predictions of medial tibiofemoral contact forces. J. Biomech. 46, 2778–2786.
Geyer, H., Herr, H., 2010. A muscle-reflex model that encodes principles of legged mechanics produces human walking dynamics and muscle activities. IEEE Trans. Neural Syst. Rehabil. Eng. 18, 263–273.
Goffe, W.L., Ferrier, G.D., Rogers, J., 1994. Global optimization of statistical functions with simulated annealing. J. Econom. 60, 65–99.
Hamner, S.R., Delp, S.L., 2013. Muscle contributions to fore-aft and vertical body mass center accelerations over a range of running speeds. J. Biomech. 46, 780–787.
Hamner, S.R., Seth, A., Delp, S.L., 2010. Muscle contributions to propulsion and support during running. J. Biomech. 43, 2709–2716.
Higginson, J.S., Ramsay, J.W., Buchanan, T.S., 2012. Hybrid models of the neuromusculoskeletal system improve subject-specificity. Proc. Inst. Mech. Eng. Part H J. Eng. Med. 226, 113–119.
Krishnaswamy, P., Brown, E.N., Herr, H.M., 2011. Human leg model predicts ankle muscle-tendon morphology, state, roles and energetics in walking. PLoS Comput. Biol. 7, 1–16.
Kumar, D., Rudolph, K.S., Manal, K.T., 2012. EMG-driven modeling approach to muscle force and joint load estimations: case study in knee osteoarthritis. J. Orthop. Res. 30, 377–383.
Latash, M.L., 2010. Motor synergies and the equilibrium-point hypothesis. Motor Control 14, 294–322.
Leroux, A., Fung, J., Barbeau, H., 2002. Postural adaptation to walking on inclined surfaces: I. Normal strategies. Gait Posture 15, 64–74.
Liu, M.Q., Anderson, F.C., Schwartz, M.H., Delp, S.L., 2008. Muscle contributions to support and progression over a range of walking speeds. J. Biomech. 41, 3243–3252.
Lloyd, D.G., Besier, T.F., 2003. An EMG-driven musculoskeletal model to estimate muscle forces and knee joint moments in vivo. J. Biomech. 36, 765–776.
Manal, K., Buchanan, T.S., 2013. An electromyogram-driven musculoskeletal model of the knee to predict in vivo joint contact forces during normal and novel gait patterns. J. Biomech. Eng. 135, 0210141–0210147.
Manal, K., Gonzalez, R.V, Lloyd, D.G., Buchanan, T.S., 2002. A real-time EMG-driven virtual arm. Comput. Biol. Med. 32, 25–36.
Menegaldo, L.L., Oliveira, L.F., 2011. An EMG-driven model to evaluate quadriceps strengthening after an isokinetic training. Procedia IUTAM 2, 131–141.
Modenese, L., Phillips, A.T.M., 2011. Prediction of hip contact forces and muscle activations during walking at different speeds. Multibody Syst. Dyn., 157–168.
Norton, J.A., Gorassini, M.A., 2006. Changes in cortically related intermuscular coherence accompanying improvements in locomotor skills in incomplete spinal cord injury. J. Neurophysiol. 95, 2580–2589.
Salvador, S., Chan, P., 2005. Learning states and rules for detecting anomalies in time series. Appl. Intell. 23, 241–255.
Sartori, M., Gizzi, L., Lloyd, D.G., Farina, D., 2013. A musculoskeletal model of human locomotion driven by a low dimensional set of impulsive excitation primitives. Front. Comput. Neurosci. 7, 79. http://dx.doi.org/http://dx.doi.org/10.3389/fncom.2013.00079.
Sartori, M., Reggiani, M., Farina, D., Lloyd, D.G., 2012a. EMG-driven forward-dynamic estimation of muscle force and joint moment about multiple degrees of freedom in the human lower extremity. PLoS One 7, 1–11.
Sartori, M., Reggiani, M., van den Bogert, A.J., Lloyd, D.G., 2012b. Estimation of musculotendon kinematics in large musculoskeletal models using multidimensional B-splines. J. Biomech. 45, 595–601.
Seth, A., Pandy, M.G., 2007. A neuromusculoskeletal tracking method for estimating individual muscle forces in human movement. J. Biomech. 40, 356–366.
Shao, Q., Bassett, D.N., Manal, K., Buchanan, T.S., 2009. An EMG-driven model to estimate muscle forces and joint moments in stroke patients. Comput. Biol. Med. 39, 1083–1088.
Tax, A.A., Denier van der Gon, J.J., Erkelens, C.J., 1990. Differences in coordination of elbow flexor muscles in force tasks and in movement tasks. Exp. Brain Res. 81, 567–572.
Thelen, D.G., Anderson, F.C., 2006. Using computed muscle control to generate forward dynamic simulations of human walking from experimental data. J. Biomech. 39, 1107–1115.
Thelen, D.G., Anderson, F.C., Delp, S.L., 2003. Generating dynamic simulations of movement using computed muscle control. J. Biomech. 36, 321–328.
Walter, J., Kinney, A.L., Banks, S.A., D'Lima, D., Besier, T.F., Lloyd, D.G., Fregly, B.J., 2014. Muscle synergies may improve optimization prediction of knee contact forces during walking. J. Biomech. Eng. 136, 9.
Wang, J.M., Hamner, S.R., Delp, S.L., 2007. Optimizing Locomotion Controllers Using Biologically-Based Actuators and Objectives.
Winby, C.R., Lloyd, D.G., Kirk, T.B., 2008. Evaluation of different analytical methods for subject-specific scaling of musculotendon parameters. J. Biomech. 41, 1682–1688.
Winter, D.A., 2009. Biomechanics and Motor Control of Human Movement, fourth ed. John Wiley and Sons, Inc., Hoboken, New Jersey.